ADVANCED FUNCTIONAL MATERIALS
www.afm-journal.de

Snake-Inspired, Nano-Stepped Surface with Tunable Frictional Anisotropy Made from a Shape-Memory Polymer for Unidirectional Transport of Microparticles

*Weibin Wu, Markus Guttmann, Marc Schneider, Richard Thelen, Matthias Worgull, Guillaume Gomard, and Hendrik Hölscher**

The ventral scales of many snake species are decorated with oriented micro-fibril structures featuring nano-steps to achieve anisotropic friction for efficient locomotion. Here, a nano-stepped surface with tunable frictional anisotropy inspired by this natural structure is presented. It is fabricated by replicating the micro-fibril structure of the ventral scales of the Chinese cobra (*Naja atra*) into a thermo-responsive shape-memory polymer via hot embossing. The resulting smart surface transfers from a flat topography to a predefined structure of nano-steps upon heating. During this recovery process, the nano-steps grow out of the surfaces resulting in a surface with frictional anisotropy, which is characterized in situ by an atomic force microscopy. The desired frictional anisotropy can be customized by stopping the heating process before full recovery. The nano-stepped surface is employed for the unidirectional transport of microscale particles through small random vibrations. Due to the frictional anisotropy, the microspheres drift unidirectionally (down the nano-steps). Finally, dry self-cleaning is demonstrated by the transportation of a pile of microparticles.

1. Introduction

Several animals and plants ingeniously developed anisotropic micro- or nanostructures to facilitate smart functions.[1] Prominent examples include butterfly wings[2] and rice leaves[3,4] featuring directional superhydrophobicity, or slippery peristomes of *Nepenthes* pitcher plants.[5] These natural prototypes inspired the development of artificial surfaces with unidirectional wetting properties allowing the transport of liquid droplets.[4,6,7] Another interesting case is the frictional anisotropy of snake scales[8–13] enabling snakes to locomote efficiently, even on slippery or inclined surfaces. While some snakes use the edges of their ventral scales to climb even trees,[10] many snakes feature oriented micron-sized fibrils with nanoscale steps causing anisotropic friction along their body (**Figure 1**a).[13–18]

Embedding this anisotropic frictional capability in engineered surfaces promises great potential for applications which demand frictional anisotropy. Consequently, several artificial surfaces have been designed and fabricated through replicating the arrangement of snake scales on metal[19,20] or by mimicking the micro-fibril structure with polymers,[21,22] metals,[23,24] or even ceramics.[25] And indeed, frictional anisotropy was demonstrated on these snake-inspired, micro-structured surfaces.

Here, we go a step further and present a smart surface which can reversibly switch between isotropic and anisotropic friction or even tune the frictional anisotropy (Figure 1b). For that purpose we utilize the unique properties of shape memory polymers (SMPs)[26,27] which "memorize" a predefined so-called permanent shape. Once this permanent shape is defined, they can be manipulated into nearly any arbitrary, so-called temporary shape in a programming process. Afterward, they switch back to the memorized permanent shape in a recovery process if triggered by an external stimulus such as heat or light.[28–32] Recent studies also reported on SMPs with recovery triggers such as electric[33] and magnetic[34] excitations as well as humidity.[35,36] This intrinsic material property of SMPs together with the possibility to structure their surface down to the nanoscale provides great potential for the development of smart surfaces with switchable functionality. So far, SMPs have been successfully prepared with various microstructures including elements for optics,[37–39] medicine,[40] wetting control,[4,41–43] and reversible adhesion.[44–47]

Dr. W. Wu, Dr. M. Guttmann, M. Schneider, R. Thelen, Dr. M. Worgull, Dr. G. Gomard, Dr. H. Hölscher
Institute of Microstructure Technology (IMT)
Karlsruhe Institute of Technology (KIT)
H.-v.-Helmholtz-Platz 1, 76344 Eggenstein-Leopoldshafen, Germany
E-mail: hendrik.hoelscher@kit.edu

Dr. W. Wu
Institute of Noise and Vibration
Naval University of Engineering
Wuhan 430033, P. R. China

Dr. G. Gomard
Light Technology Institute (LTI)
Karlsruhe Institute of Technology (KIT)
Engesserstrasse 13, 76131 Karlsruhe, Germany

The ORCID identification number(s) for the author(s) of this article can be found under https://doi.org/10.1002/adfm.202009611.

DOI: 10.1002/adfm.202009611

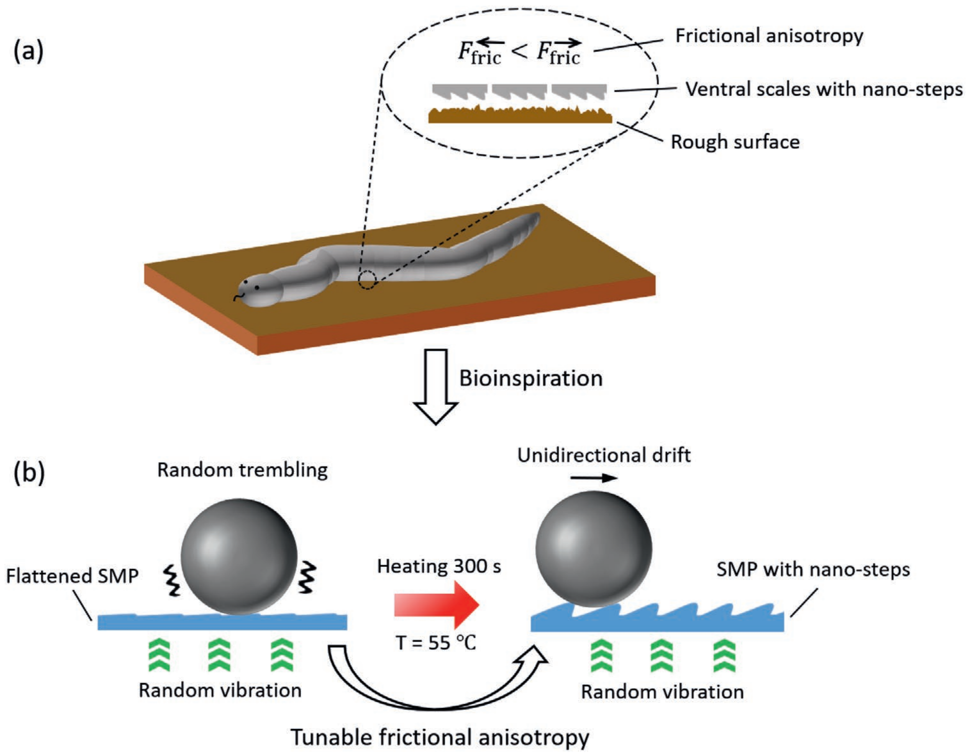

Figure 1. a) Schematic of a snake in direct contact with the ground. Since its scales are equipped with nanoscale steps, they exhibit frictional anisotropy. Therefore, movement in forward direction is easier than in backward direction. b) Schematic representation of the snake-inspired, nano-stepped surface. The structure is replicated into a shape memory polymer (SMP), which can be switched from a flat to a nanostructured surface via heating. For the unidirectional transport experiments, one or more microparticles are put on top of the surface in both states. When the surface is flat, the random vibration of the surface causes only a trembling of the particles. After heating, nano-steps grow out of the surface causing frictional anisotropy. As a result, the particles drift in the direction of lower friction. Please note that the schematic is not to scale, that is, the height of nanosteps of a snake scale is well-below 100 nm while the periodicity is in the range 3–5 µm (see Figures 2 and 3 as well as ref. [13])

Our smart surface is fabricated by replicating the micro-fibril structures found on the ventral scales of the Chinese cobra (*Naja atra*) into a SMP foil. The magnitude of friction anisotropy on the surface can be controlled by tuning the height of nano-steps at the fibril tips during recovery. The step height as well as the induced frictional anisotropy at the nano-steps during the recovery process are characterized in situ by atomic force microscopy (AFM). The long-term stability of the height of the nano-steps was monitored at four different stages of the recovery process. The reusability is proven by the analysis of flattening/recovery cycles. Finally, the resulting smart surface is utilized for the unidirectional transport of single microspheres made from polydimethylsiloxane (PDMS). Further experiments showing the simultaneous transport of many PDMS microspheres and sand particles demonstrate the potential for dry self-cleaning of technical surfaces.

2. Results and Discussion

2.1. Snake Inspired Surface with Switchable Topography

As outlined in Figure 1 we use the ventral scales of snakes as an inspiration to fabricate a smart surface from a SMP whose surface can be switched from a flat to a nano-stepped configuration. **Figure 2** summarizes the whole process. Figure 2a–c displays the replication of the micro-fibril structures from the ventral scale of the Chinese cobra into a SMP foil. We chose this species because it features a comparable high frictional anisotropy.[13] The mold (Ni-shim) fabricated by nickel plating of a snake scale features a negative pattern of the micro-fibril structures as shown by the scanning electron microscopy (SEM) image in Figure 2b. The resulting replication quality of the SMP foil embossed at $T > T_{hard}$ is demonstrated by the SEM image in Figure 2c. The snake scale and the structured SMP surface have the same micro-fibril structure. The translucent area on the transparent SMP foil in Figure 2c indicates the existence of microstructures on the surface. Through pressing with a flat silicon wafer at a temperature higher than T_{switch} (but below T_{hard}), the structured SMP surface is programmed into a so-called temporary state with a smooth topography (Figure 2d). In this step, the half-opaque area also becomes transparent revealing the flattening of the micro-fibril structure which is also shown in more detail by the respective SEM image. Please note that this state—although commonly named "temporary"—is stable as long as the foil is stored well-below T_{switch} as shown in Figure S3a, Supporting Information. Therefore, only heating, with a hot plate for example, causes the growth of the micro-fibril structure leading to half-opaque surface again (Figure 2e). The respective SEM image confirms the recovery of the micro-fibril structure. In this way, the SMP surface can be reversibly

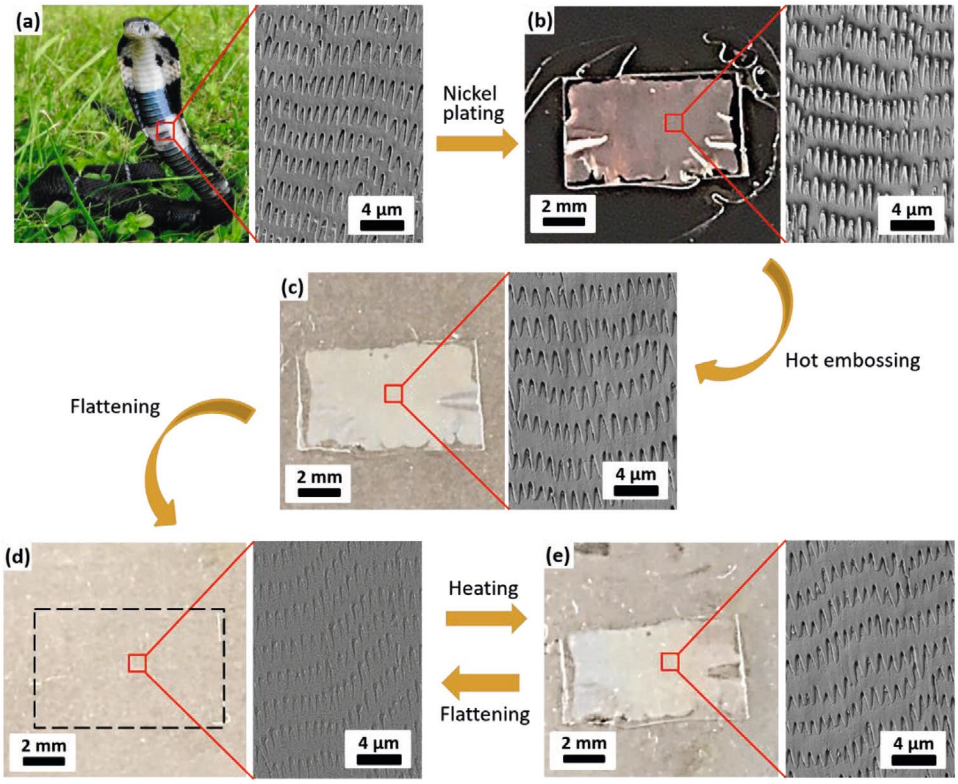

Figure 2. Photographs of the Chinese cobra, a Ni-shim and a replicated SMP foil in its different shapes together with corresponding SEM images showing the respective surface topography. a) Photo of a Chinese cobra (photo by Guillaume Gomard, used with permission). The SEM image of a ventral scale reveals the oriented micro-fibril structure. b) Nickel shim fabricated by electroplating of a singled and cut ventral scale. The negative pattern of the micro-fibril structures is revealed in the SEM image. c) The SMP surface replicated with the shim shown in (b) results in the same type of micro-fibril structure displayed in (a). d) After flattening the SMP surface with a flat silicon wafer the structured area disappears. The respective SEM image shows the flattened surface, the edges of the fibrils, however, are still visible. e) After heating the flattened SMP foil at 55 °C, the original fibril structure with nano-steps recovers. Flattening and heating can be repeated, allowing to switch the topography between flat (d) and structured (e) many times.

switched between the flattened and structured topography by cyclically conducting the flattening and heating processes.

2.2. In Situ Characterization of Topography and Friction Anisotropy by Atomic Force Microscopy

AFM allows the in situ characterization of the restoring process of the SMP foil. **Figure 3**a–c shows the respective AFM images during the transformation from a flattened to a recovered, structured surface at the same location of a SMP foil. The bottom panels display the topographical line sections along the red, dashed arrows in the upper AFM images. A roughly flat topography is observed over the 10 µm scan range in Figure 3a. The edges of the steps are still observable, but their heights are less than 6 nm. After heating the sample on a hot plate for 10 s, the topography at the same position changes significantly as shown in Figure 3b. The line section across the same fibrils already shown in Figure 3a reveals that the step heights increase to more than 30 nm. Further heating causes a complete recovery of the surface after 200 s (Figure 3c). The step heights of the same fibrils as shown in Figure 3b increase to almost 60 nm. Furthermore, it is interesting to note that the overall shape of the fibrils remains unchanged during this recovery process while their length and width reduce slightly.

We also analyzed the growth process of the single fibril step marked by the black arrow in Figure 3a–c. Figure 3d displays seven height measurements taken during the complete heat induced recovery process as a function of time. The data points are close to a straight line if plotted on a logarithmic time scale. The same result is observed at other steps of micro-fibrils (see Figure S2a, Supporting Information). This confirms that the height increases exponentially with heating time at a fixed temperature, as already described in refs. [37,48].

AFM has the advantage that the frictional forces at the nano-steps can be measured simultaneously with the topography during the recovery process. Figure 3e shows the friction loops of the AFM tip scanning the fibril steps up (trace direction) and down (retrace direction) along the position marked as a red, dashed line in the topography images in Figure 3a,c, respectively. As frequently observed, there is a significant frictional peak marked by arrows at the nanoscale step edges for upward scans and a smaller one for downward scans.[13,17,49] A comparison of the two friction loops reveals also that the frictional peak for the upward scans is much higher for the structured (Figure 3c) than for the flattened surface (Figure 3a). For downward scans, however, the frictional peaks for the two cases are almost equivalent. Consequently, there is a large difference between upward and downward scans for the structured surface leading to a frictional anisotropy. For the flattened surface,

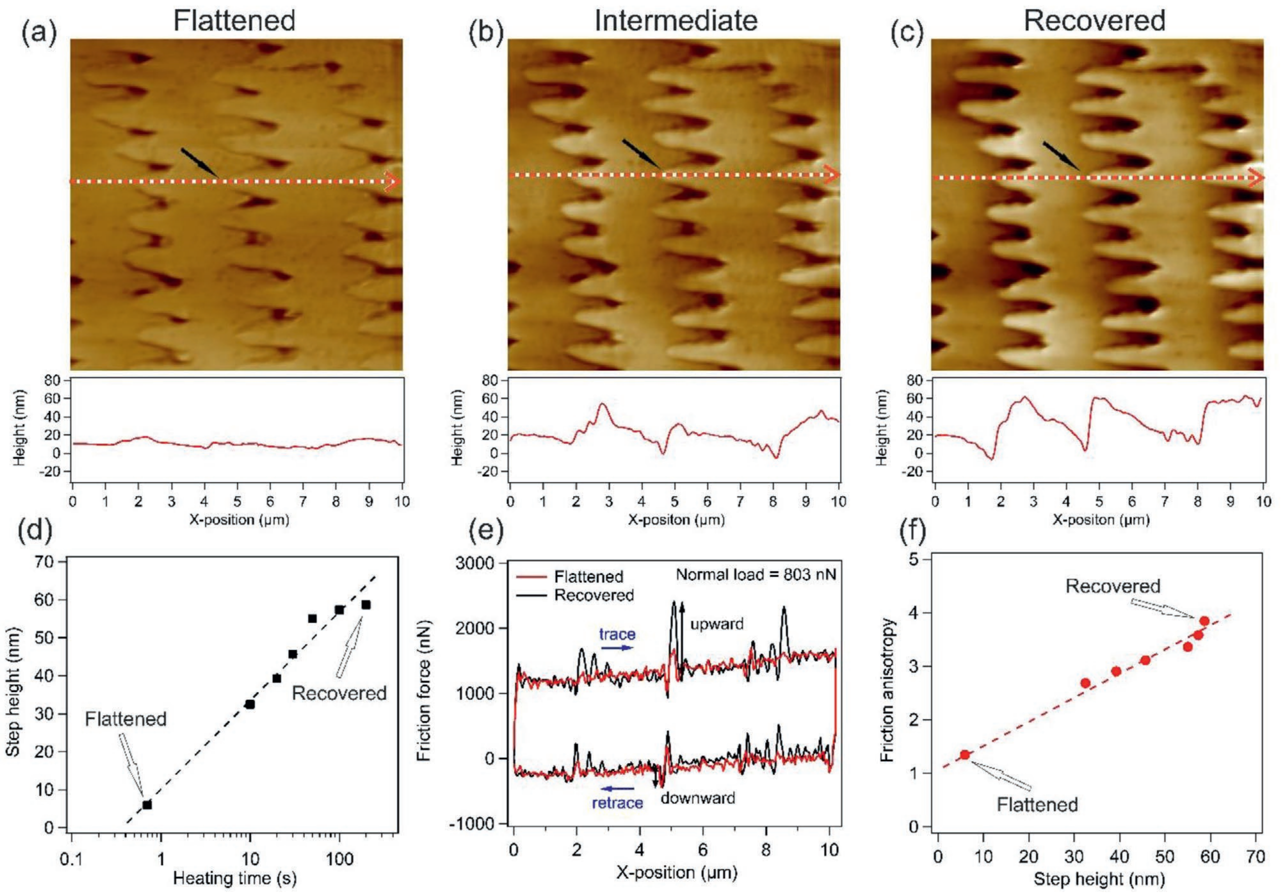

Figure 3. Analysis of the recovery of a temporarily flattened SMP foil to its permanent, structured topography by heating. The evolution of step height and friction anisotropy at micro-fibril ends during this process were characterized in situ by AFM. a) An AFM image of the flattened micro-fibrils before heating. The bottom panel shows the topographical line section (along the red arrow in the AFM image) across the fibril ends revealing less than 6 nm step heights. b) The same measurement as in (a) after heating the SMP foil for 10 s. During measurements the heating was stopped. The topographical line section shows that the step height of the fibril tips increased to some 30 nm. c) After 200 s heating time, the AFM image and line section indicate that the step heights increased to nearly 60 nm. d) The evolution of the step height versus heating measured at the fibril end marked by an arrow in the AFM image. The first and last data point correspond to the AFM images shown in (a) and (c). e) The friction loop of the AFM tip scanning across the same fibrils (along the red arrow in the AFM image) for both upward and downward the step directions on the flattened and recovered surface shown in (a) and (c), respectively. The normal load in both cases was 803 nN. A large frictional peak (marked by the black arrows) was observed at the fibril steps. When the AFM tip stepping up the fibrils (trace), the frictional increase on the recovered surface is much larger than that on the flattened one, while for stepping down direction (retrace) the frictional increase on the two surfaces are almost equivalent. This indicates larger friction anisotropy on the recovered surface than on the flattened surface. f) The calculated friction anisotropy at the second fibril end (marked by an arrow in the AFM image) is plotted as a function of its corresponding step height during the recovery process from (a) to (c). A nearly linear relationship is observed.

however, the anisotropic effect is almost negligible. This outcome is in agreement with other studies showing that frictional anisotropy of snake scales can be detected by AFM,[13,17] tribometry[50] as well as by classical friction experiments with an inclined plane.[51,52]

Figure 3f displays the frictional anisotropy at the second fibril step (marked by the black arrow in the AFM images) as a function of the corresponding step height during the surface recovery process. Altogether, we were able to measure seven data points during the recovery from the flattened (Figure 3a) to the structured surface with a step height of about 60 nm (Figure 3c). In accordance with our previous observation on snake scales (see Figure 3 in ref. [13]), the frictional anisotropy increases almost linearly with the step height. The initial frictional anisotropy on the temporarily flattened surface (Figure 3a) was close to one (1.35) and finally increased to 3.84 after full recovery (Figure 3c). Additional measurements of the frictional anisotropy at two other micro-fibril steps are plotted in Figure S1b, Supporting Information. All data points fit to a straight line. This outcome proofs that the frictional anisotropy increases linearly with the height of the nano-steps which in turn can be controlled via the heating time of the SMP foil.

This result suggests that the frictional anisotropy can be set through the step-height which can be controlled by stopping the recovery process at the dedicated value. Thus, we produced several samples, stopped their recovery at various states, stored them under controlled conditions well below T_{switch} and analyzed their topography weekly over a time span of three months. The step heights stayed constant within the experimental error for 12 weeks (see Figure S3a, Supporting Information). Additionally, we analyzed the step heights during eleven consecutive flattening and recovery cycles and observed no degrading within the experimental error (see Figure S3b, Supporting Information). Furthermore, it might be interesting to note that the optical transmittance of the polymer foils is about 90% in the visible range for flat as well as for the structured surface (see Figure S4, Supporting Information) because the overall height of the nano-steps is one order of magnitude smaller than the visible wavelengths.

2.3. Drift of Microparticles through Random Vibrations

As already outlined in Figure 1b it is the goal of our study to utilize the snake inspired surfaces for the transport of microparticles. The approach is based on the fact that a small particle on top of a laterally vibrated surface with frictional anisotropy experiences a net force acting in the direction of lower friction. A simplified but instructive model is presented in Figure S1, Supporting Information.

Figure 4 visualizes the directional drift of small particles transported due to this effect on several samples. A ventral scale of the Chinese cobra served as reference and is compared with three artificial surfaces: An originally structured SMP, a flattened one, and a recovered one. All examined surfaces were sputter-coated with a thin homogeneous silver layer to increase visibility of the microparticles under the light microscope and to achieve similar surface properties for all samples. Furthermore, the metallic layer avoids possible triboelectric effects. After placing a PDMS microsphere on each surface, we vibrated the surfaces with a small vibration motor and recorded the particles' movement with an optical microscope.

Figure 4a demonstrates the drift of a PDMS microsphere on the vibrated snake scale. The left image displays the starting position of the sphere. The SEM image in the inset shows the surface structure and indicates the orientation of the micro-fibrils pointing from top to bottom. With the onset of the vibrations, the microparticle starts to tremble in all directions, but due to the frictional anisotropy of the snake scale, the movement in bottom direction is slightly easier. Consequently, it performs small random jumps in all directions, but the overall drift is largest along the micro-fibril structure to the bottom of the image. The center and right optical image reveals the position of the sphere after 11 and 14 s. The complete path is plotted by data points in the graph on the right. Within 43 s the drift in y-direction is about 5.5 mm while the random movement in x-direction does not exceed 0.5 mm.

The overall phenomenon is also observed on the structured SMP foils. Putting other PDMS microspheres on the originally structured (Figure 4b) and recovered SMP foil (Figure 4d) we observe a clear drift of each particle along the direction of the micro-fibrils (to the bottom in our presentation) due to the vibration of the surfaces. The respective travelling distances in y- and x-direction on these two surfaces are 4.3 and 0.26 mm (time span 20 s) and 4.75 and 0.45 mm (time span 41 s), respectively. We would like to point out that the overall movement is a stochastic path due to the random mechanical vibrations. Furthermore, we used microspheres with slightly different diameters in Figure 4. Consequently, the overall drift velocities cannot be compared directly. The net drift, however, is unidirectional and the significant travel distance is only observed on the structured surfaces. Repeating the experiment on a completely flat surface or a flattened SMP foil results in a trembling of the respective sphere under observation but the overall long-term drift is negligible as demonstrated by the photographs and the plot in Figure 4c. Videos of the experiments summarized in Figure 4 are available in the Videos S1–S4, Supporting Information.

2.4. Dry Self-Cleaning with Snake Scale Inspired Surfaces

From the above presented experiments, we conclude that the surface structure of snakes can be copied to artificial surfaces which exhibit the same frictional anisotropy as snake scales. Moreover, this anisotropy can be switched on and off if replicated into a shape memory polymer. As a result, small particles can be artificially forced to drift in a predefined direction if the surface is mechanically excited by small vibrations.

This forced drift can be also applied to clean such a snake inspired surface from microparticles like dust or dry soil. **Figure 5** shows such dry self-cleaning experiments. In order to demonstrate that the orientation of the micro-fibrils determines the direction of the drift, we placed two uniform samples of structured SMP foils in opposite direction on top of the vibration motor, that is, the micro-fibrils point to the left for the left surface and to the right for the right one. Consequently, the frictional anisotropy of the two samples points in opposite directions.

Figure 5 summarizes the drift experiments conducted with this set-up. As a control experiment, we first placed two microspheres close to the center of the two samples and started the random vibration. As expected, they drift in opposite direction and reach the left and right borders of the two samples within 7 s (left column of Figure 5 and Video S5, Supporting Information). In order to demonstrate that piles of similar microparticles are also transported unidirectionally, we placed several microspheres and sand grains in the stitching of the two surfaces (middle and right column of Figure 5 and Videos S6,S7, Supporting Information). After the start of the random vibration, the complete area is cleaned within 65 and 105 s for the microspheres and sand grains, respectively. In general, we observed that different types of particles which differ in size and material drift at different velocities. We therefore conclude that the cleaning process for the sand grains took longer time than for the microspheres. This feature opens the opportunity to separate particles through their different drift rate.

3. Conclusion and Outlook

To conclude, we developed a smart surface with anisotropic frictional properties inspired by the micro-fibril structure of snake scales allowing to transport microparticles through small random vibrations. As the smart surface is fabricated from a shape memory polymer it can be switched between a flattened and a micro-fibril structured topography with nanoscale steps upon heating and flattening. Accordingly, the frictional properties of the surface change from nearly isotropic to

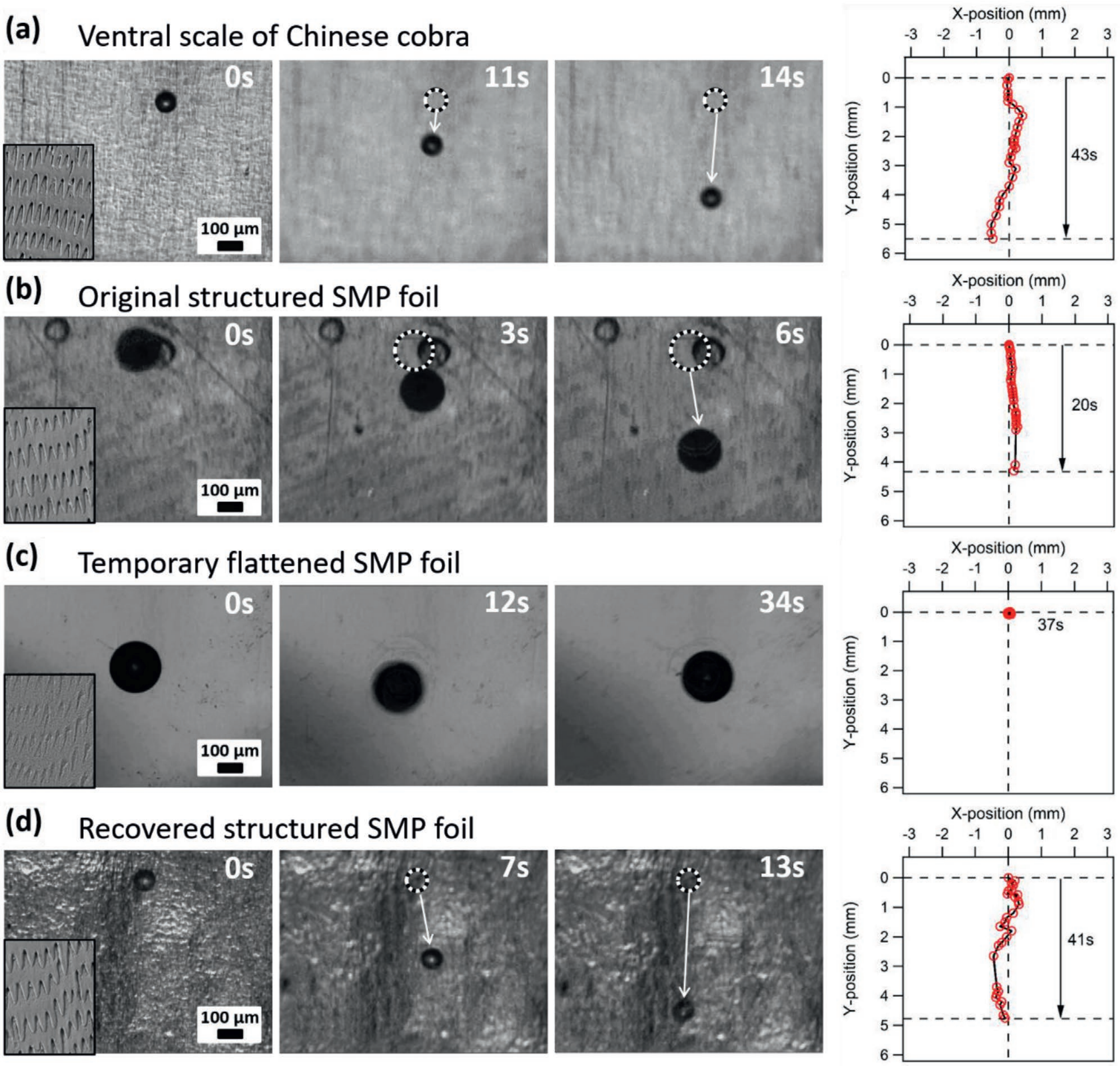

Figure 4. Movement of PDMS microspheres with slightly different diameters on a vibrated a) ventral scale of Chinese cobra, b) original structured, c) temporarily flattened, and d) recovered SMP foil. The photographs in the first three columns show the time-lapse of the microsphere drifting on the different substrates. The SEM images in the insets indicate the orientation of micro-fibril structures on the surfaces. They point always toward the bottom. The dashed circles in (a, b and d) represent the original position of the microspheres. The line charts in the last column mark the tracked trajectory of the microsphere travelling on the corresponding substrate for many seconds. The microsphere drifts in the direction of the fibrils (downward in this representation) in (a, b and d) but no drift was observed in (c) on the flattened SMP foil. About 30 data points were plotted for each trajectory, the time intervals between the data points are not alike. All surfaces were sputter-coated with a 10 nm silver layer to increase visibility (see experimental section).

anisotropic along the fibril direction. Since the frictional anisotropy increases linearly with the step height, it can be controlled by interrupting the recovery process at any intermediate step height. The SMP foils show excellent long-term stability and reusability. The anisotropy of the surface can be utilized for the unidirectional transport of microparticles through random vibration of the samples. The simultaneous transport of complete layers of microspheres or sand particles demonstrates dry self-cleaning.

The presented approach is different to previous studies where various actuation mechanisms ranging from sound[53,54] to magnetic[55,56] or UV light stimulation[57] were utilized for the directional transport of micro-objects such as liquid droplets,[56] microspheres,[54,55,57] a polymer sheet,[54] and a hydrogel rod.[53] However, most of them were achieved by surface anisotropy due to a ratchet like surface or flexible microstructures impacting the micro-objects on top of the respective surface. In the case presented here, the height of the surface structures is

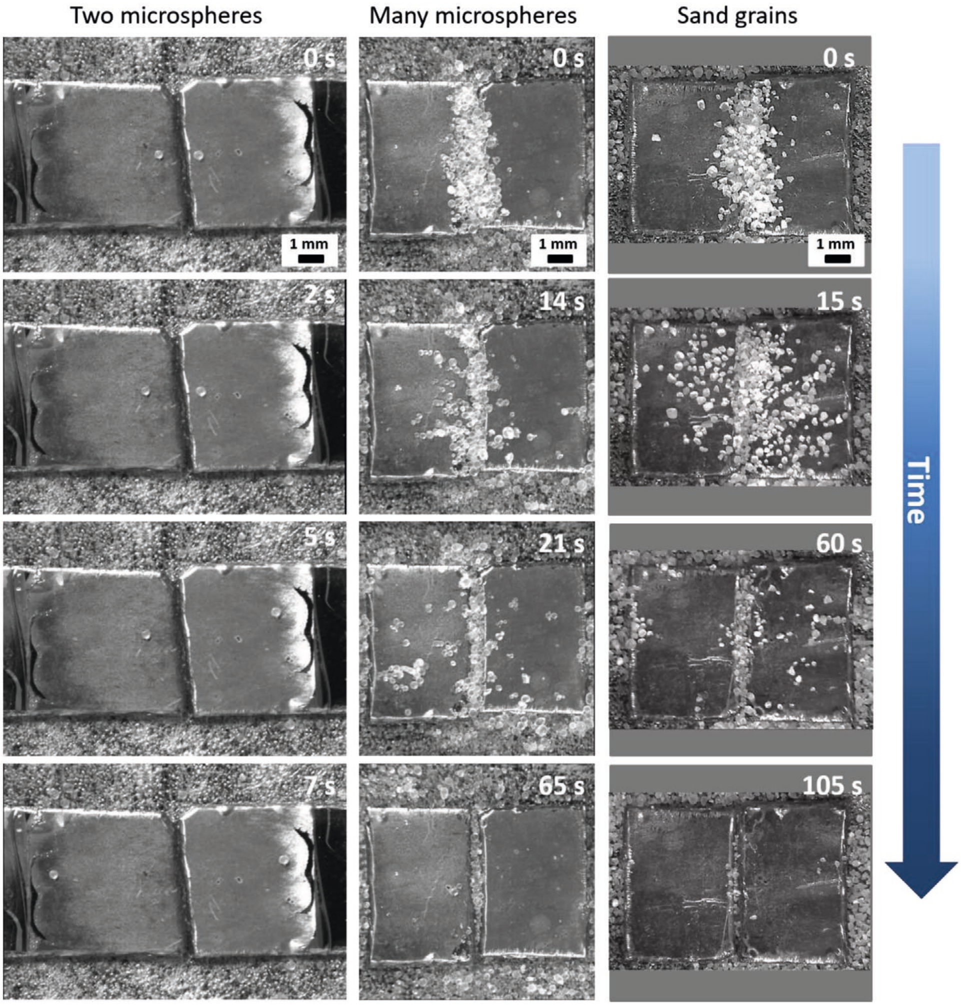

Figure 5. Simultaneous transportation of PDMS microspheres and sand grains on two structured SMP foils where the nano-steps are in opposite direction, that is, the micro-fibril structures on the left and right SMP foil point toward left and right, respectively. The left column displays the drift of two single PDMS microspheres. The transportation of many microspheres and sand grains is displayed in the middle and right column, respectively. All particles with slightly different diameters were initially placed at the center of the two foils. Subsequent vibration of the substrate caused the separation of the respective particles toward the left and right (corresponding to the fibril step direction). This effect can be used for the dry self-cleaning of surfaces. Movies of the drifting particles can be found in the Supporting Information.

well below 100 nm while their periodicity is some µm. Consequently, the polymer foils have a high transmittance and appear transparent to the naked eye.

Due to these favorable optical properties, we speculate that snake scale inspired surfaces might be applied for the dry self-cleaning of technical surfaces. Possible applications include photovoltaic modules which are installed in extreme dry areas with many sun hours. Here, the lack of rain coincides with numerous sun hours but at the same time the removal of dust and dry soil is an issue.[58] Cleaning with water needs costly manpower or robots and might cause other issues.[58] In such a case, the dry self-cleaning through mechanical vibrations seems a promising approach.

Nonetheless, further studies are necessary to exploit the limits of the directional transportation through frictional anisotropy as well as optimized parameters for the respective technical application. The distance between the nanosteps and their height will influence the magnitude of the directional transport through frictional anisotropy. As soil and dust are not alike worldwide further tests in the field are necessary to evaluate the applicability of dry self-cleaning, that is, it might be necessary to use dedicated topography parameters for each region.

Further applications might include sorting particles by different drift rate. Since the average drift rate correlates with the frictional anisotropy, particles with different tribological properties might be separated through the presented mechanism.

4. Experimental Section

Nickel Shim Fabrication: To replicate the micro-fibril structures of snake scales into SMP surfaces via hot embossing, robust nickel shims with negative patterns of the nano-stepped micro-fibrils were fabricated. For that, molted ventral scales of *N. atra* (provided by Guillaume Gomard) were cut into rectangles with a size of 10 × 7 mm and then blown with pressurized air for around 5 s to clean them from possible contaminations. The scales prepared in this way were glued with Norland Optical Adhesive 88 (Norland Products, Inc. USA) onto a 4-inch silicon wafer and evaporated with 8 nm of chromium (adhesive layer) and 40 nm of gold (conductive plating base). Subsequently, the substrate was masked with nonconductive tapes leaving a circular plating window with a diameter of 85 mm defining the final Ni-shim size. After that, the masked substrate was mounted to a special plating holder and immersed into the standard electroplating system with a boric acid containing nickel sulfamate electrolyte ($T = 52$ °C, pH 3.4–3.6).[59] During the plating process, the current density was gradually increased from 0.1 to 1 A·dm^{-2} to slowly fill the micro-structured areas. This process results in a defect-free, stiff homogenous nickel layer with a thickness of about 600 µm, which could repeatedly endure forces of several tens of kilo-Newton in the following hot embossing process. Next, the silicon wafer was removed by dissolving it in 30% KOH solution and the snake scales together with the glue were eliminated from the thick nickel layer using chloroform in an ultrasonic bath (at 40 °C for 30 min). Finally, the obtained Ni-shim with negative micro-fibril structures was mechanically cut into a disk with 78 mm diameter and cleaned by oxygen plasma (STP2020, R3T, Germany) for 60 min at 22 °C, 800 W, 450 mTorr.

Defining and Manipulating the Topography of the Smart Surface: The shape memory polymer used in this study was the thermally triggered, cycloaliphatic polyether urethane block copolymer distributed as Tecoflex EG-72D (Lubrizol Corp., USA). Its permanent shape could be defined while synthesizing or redefined after fabrication by melting when the temperature was over the transition temperature T_{hard}. To program a temporary shape, the temperature should be higher than the switching temperature T_{switch} of the SMP but below its transition temperature T_{hard}. Cooling the polymer after deformation, the temporary shape was obtained and will be stable as long as the temperature was below T_{switch}. The recovery process happened only if the polymer was heated to (or close to) T_{switch}. Then, it would continuously recover back to its original permanent shape. In previous studies[37,39,60–63] with the same SMP, the temperatures $T_{hard} \approx 150$ °C and $T_{switch} \approx 40–70$ °C were determined.

The hot embossing technique was applied to structure the SMP with an enhanced hot embossing machine based on a commercial system from JENOPTIK.[64,65] First, to define the permanent shape, the nano-step structure of the Chinese cobra's ventral scale was replicated into the SMP surface with a previously produced Ni-shim. For that, the shim was pressed into a foil of the SMP with an embossing force of 12 kN at a temperature of $T = 155$ °C. After cooling the foil down to room temperature, the original structured, permanent state of the smart surface was obtained. To program a temporary topography, the previously structured SMP surface was hot embossed again but with a flat silicon wafer (used as mold) with an embossing force of 8.5 kN and a temperature of 55 °C. Subsequent cooling resulted in a flat, unstructured temporary shape (or surface). Finally, placing this flat SMP foil on a hot plate (55 °C) released the inner forces and the surface recovered to its structured, permanent state again. The last two steps count as one flattening and recovery cycle of the SMP which could be repeated many times (see refs. [37,62] and Figure S2b, Supporting Information).

Characterization Methods: The topography of the snake scales, the negative structures on the Ni-shim, and the structured and flattened SMP sample were imaged by SEM (SUPRA 60 VP, Carl Zeiss AG, Germany). Sample surfaces were sputter-coated with a 10 nm thick silver layer beforehand. Microscopic friction at the nano-steps of micro-fibril tips was characterized with a Dimension Icon AFM (Veeco Inc., USA) in contact mode. Normal load and lateral force were calibrated following the procedure proposed by Schwarz et al.[66] by adopting spring constant and deflection sensitivity of the AFM cantilever (All-in-One-Al, BudgetSensors Ltd., Bulgaria) with the help of integrated AFM software. The frictional anisotropy was calculated as described in ref. [13]. The normal load on the surface was increased and recorded the frictional increase at the fibril steps. Friction coefficients for scanning the AFM tip upward (μ_{up}) and downward (μ_{down}) the fibril step were calculated from respective linear fits of the data.[49] Frictional anisotropy was defined as the coefficient between upward and downward scans (μ_{up}/μ_{down}).[13] The scan size was set to 10 µm × 10 µm. To analyze the long-term stability and reusability of the SMP samples, the height of the nano-steps at micro-fibril tips was measured by AFM in tapping mode (scan size: 15 µm × 15 µm). Five different positions were measured on each sample with eight step heights evaluated on each position. The averaged step height was calculated from a total of $5 \times 8 = 40$ data points and the corresponding standard deviation was plotted as error bars in the respective graphs. All samples were stored in a refrigerator with a constant temperature of 4 °C and measured in temperature (21–23 °C) and humidity (50–70%) controlled environment.

Drift Experiments: Snake scales as well as flat and structured SMP foils were glued on a silicon substrate with double-sided adhesive tape (Fotostrip, Tesa AG, Germany) and sputter-coated with a 10 nm silver layer. This sputtering process did not affect the resulting height of the fibrils because the surface was evenly covered with silver as confirmed by AFM. The thin metal layer had some advantages for the subsequent drift analysis. It increased the visibility of the microspheres and avoided possible tribo-electricity between the SMP foil and the utilized PDMS spheres. The silicon substrate was fixed on a commercial coin-type vibrating motor for mobile phones. Its working principle is based on an eccentric rotating mass (Brunswick Corporation, USA). It has a diameter of 10 mm and a thickness of 2.7 mm. Its nominal voltage and current are 1.5 V and 0.05 A, respectively. The measured ground frequency was about 110 Hz with overtones at 220and 330 Hz together with a forest of higher frequencies. The whole setup was then mounted on a microscope slide with double-sided adhesive tape and fixed on the stage of an optical microscope (ProMicron GmbH, Germany) with sticky tape. PDMS microspheres (100–200 µm diameter) or micro sand particles (100–300 µm diameter, Merck KGaA, Germany) were selected and positioned on the sample surface with a tweezer. This size is close to many dirt particles. Furthermore, these sizes allowed to observe a reasonable drift path related to the size of the snake scales and could be easily tracked by optical microscopy during the dry self-cleaning experiments. The vibrating motor was powered by a voltage and current adjustable power supply (E3620A, Agilent Technologies Inc., UK). The movement of the microparticles was tracked and recorded with a computer connecting to the microscope. Afterward the paths were analyzed by the Motion Tracking Function in Corel VideoStudio Pro 2020.

Supporting Information

Supporting Information is available from the Wiley Online Library or from the author.

Acknowledgements

It is a pleasure to thank Marco Heiler, Jana Scherrer, Alexandra Moritz, and Uwe Köhler for their kind help to fabricate the Ni-shim. The authors thank Alban Muslija for the introduction into the SEM analysis and Luisa Borgmann for her kind help with the optical spectroscopy measurements. The authors also acknowledge the kind help and support of KM Samaun Reza and Patrick Weiser in the lab. W.W. gratefully acknowledges a scholarship from the China Scholarship Council (CSC). G.G. gratefully acknowledges support from the Helmholtz Postdoc Program and from the Karlsruhe School of Optics and Photonics (KSOP). This work was partly carried out with the support of the Karlsruhe Nano Micro Facility (KNMF, www.kit.edu/knmf), a Helmholtz Research Infrastructure at Karlsruhe Institute of Technology (KIT, www.kit.edu). The authors acknowledge financial support through the "Ideenwettbewerb Biotechnologie—Von der Natur lernen" of the "Ministerium für Wissenschaft, Forschung und Kunst Baden-Württemberg" (7533-7-11.10-22.)

Open access funding enabled and organized by Projekt DEAL.

Conflict of Interest

The authors declare no conflict of interest.

Data Availability Statement

Data sharing is not applicable to this article as no new data were created or analyzed in this study.

Keywords

dry self-cleaning, shape memory polymers, smart surfaces, snake scales, tunable frictional anisotropy

Received: November 10, 2020
Revised: February 4, 2021
Published online: February 28, 2021

[1] A. E. Filippov, S. N. Gorb, *Combined Discrete and Continual Approaches in Biological Modelling*, Springer, Berlin **2020**.
[2] Y. Zheng, X. Gao, L. Jiang, *Soft Matter* **2007**, *3*, 178.
[3] L. Feng, S. Li, Y. Li, H. Li, L. Zhang, J. Zhai, Y. Song, B. Liu, L. Jiang, D. Zhu, *Adv. Mater.* **2002**, *14*, 1857.
[4] Z. Cheng, D. Zhang, T. Lv, H. Lai, E. Zhang, H. Kang, Y. Wang, P. Liu, Y. Liu, Y. Du, S. Dou, L. Jiang, *Adv. Funct. Mater.* **2018**, *28*, 1705002.
[5] H. F. Bohn, W. Federle, *Proc. Natl. Acad. Sci. U. S. A.* **2004**, *101*, 14138.
[6] N. A. Malvadkar, M. J. Hancock, K. Sekeroglu, W. J. Dressick, M. C. Demirel, *Nat. Mater.* **2010**, *9*, 1023.
[7] D. Sun, K. F. Böhringer, *Microsyst. Nanoeng.* **2020**, *6*, 87.
[8] M. J. Baum, A. E. Kovalev, J. Michels, S. N. Gorb, *Tribol. Lett.* **2014**, *54*, 139.
[9] M. J. Benz, A. Lakhtakia, A. E. Kovalev, S. N. Gorb, *Proc. SPIE* **2012**, *8339*, 833901.
[10] H. Marvi, D. L. Hu, *J. R. Soc. Interface* **2012**, *9*, 3067.
[11] H. A. Abdel-Aal, M. El Mansori, H. Zahouani, *Wear* **2017**, *376*, 281.
[12] H. A. Abdel-Aal, R. Vargiolu, H. Zahouani, M. El Mansori, *J. Phys.: Conf. Ser.* **2011**, *311*, 012016.
[13] W. Wu, S. Yu, P. Schreiber, A. Dollmann, C. Lutz, G. Gomard, C. Greiner, H. Hölscher, *Bioinspir. Biomim.* **2020**, *15*, 056014.
[14] A. E. Filippov, S. N. Gorb, *Sci. Rep.* **2016**, *6*, 23539.
[15] H. A. Abdel-Aal, *J. Mech. Behav. Biomed. Mater.* **2013**, *22*, 115.
[16] H. A. Abdel-Aal, R. Vargiolu, H. Zahouani, M. El Mansori, *Wear* **2012**, *290*, 51.
[17] J. Hazel, M. Stone, M. S. Grace, V. V. Tsukruk, *J. Biomech.* **1999**, *32*, 477.
[18] W. Wu, C. Lutz, S. Mersch, R. Thelen, C. Greiner, G. Gomard, H. Holscher, *Beilstein J. Nanotechnol.* **2018**, *9*, 2618.
[19] J. Schneider, V. Djamiykov, C. Greiner, *Beilstein J. Nanotechnol.* **2018**, *9*, 2561.
[20] C. Greiner, M. Schafer, *Bioinspir. Biomim.* **2015**, *10*, 044001.
[21] M. J. Baum, L. Heepe, S. N. Gorb, *Beilstein J. Nanotechnol.* **2014**, *5*, 83.
[22] M. J. Baum, L. Heepe, E. Fadeeva, S. N. Gorb, *Beilstein J. Nanotechnol.* **2014**, *5*, 1091.
[23] P. Cuervo, D. A. López, J. P. Cano, J. C. Sánchez, S. Rudas, H. Estupiñán, A. Toro, H. A. Abdel-Aal, *Surf. Topogr.: Metrol. Prop.* **2016**, *4*, 024013.
[24] H. A. Abdel-Aal, M. El Mansori, *Surf. Topogr.: Metrol. Prop.* **2013**, *1*, 015001.
[25] M. Mühlberger, M. Rohn, J. Danzberger, E. Sonntag, A. Rank, L. Schumm, R. Kirchner, C. Forsich, S. Gorb, B. Einwögerer, E. Trappl, D. Heim, H. Schift, I. Bergmair, *Microelectron. Eng.* **2015**, *141*, 140.
[26] A. Lendlein, S. Kelch, *Angew. Chem., Int. Ed.* **2002**, *41*, 2034.
[27] A. Lendlein, O. E. C. Gould, *Nat. Rev. Mater.* **2019**, *4*, 116.
[28] A. Lendlein, H. Jiang, O. Jünger, R. Langer, *Nature* **2005**, *434*, 879.
[29] Q. Zhao, H. J. Qi, T. Xie, *Prog. Polym. Sci.* **2015**, *49*, 79.
[30] C. Liu, H. Qin, P. T. Mather, *J. Mater. Chem.* **2007**, *17*, 1543.
[31] P. T. Mather, X. Luo, I. A. Rousseau, *Annu. Rev. Mater. Sci.* **2009**, *39*, 445.
[32] M. D. Hager, S. Bode, C. Weber, U. S. Schubert, *Prog. Polym. Sci.* **2015**, *49*, 3.
[33] J. W. Cho, J. W. Kim, Y. C. Jung, N. S. Goo, *Macromol. Rapid Commun.* **2005**, *26*, 412.
[34] R. Mohr, K. Kratz, T. Weigel, M. Lucka-Gabor, M. Moneke, A. Lendlein, *Proc. Natl. Acad. Sci. U. S. A.* **2006**, *103*, 3540.
[35] Y. Chae Jung, H. Hwa So, J. Whan Cho, *J. Macromol. Sci. B* **2006**, *45*, 453.
[36] W. M. Huang, B. Yang, L. An, C. Li, Y. S. Chan, *Appl. Phys. Lett.* **2005**, *86*, 114105.
[37] S. Schauer, T. Meier, M. Reinhard, M. Rohrig, M. Schneider, M. Heilig, A. Kolew, M. Worgull, H. Holscher, *ACS Appl. Mater. Interfaces* **2016**, *8*, 9423.
[38] H. Xu, C. Yu, S. Wang, V. Malyarchuk, T. Xie, J. A. Rogers, *Adv. Funct. Mater.* **2013**, *23*, 3299.
[39] S. Schauer, R. Schmager, R. Hünig, K. Ding, U. W. Paetzold, U. Lemmer, M. Worgull, H. Hölscher, G. Gomard, *Opt. Mater. Express* **2018**, *8*, 184.
[40] A. Lendlein, R. Langer, *Science* **2002**, *296*, 1673.
[41] D. Zhang, Z. Cheng, Y. Liu, *Chemistry* **2019**, *25*, 3979.
[42] T. Lv, Z. Cheng, D. Zhang, E. Zhang, Q. Zhao, Y. Liu, L. Jiang, *ACS Nano* **2016**, *10*, 9379.
[43] C. M. Chen, S. Yang, *Adv. Mater.* **2014**, *26*, 1283.
[44] J. D. Eisenhaure, T. Xie, S. Varghese, S. Kim, *ACS Appl. Mater. Interfaces* **2013**, *5*, 7714.
[45] L. F. Boesel, C. Greiner, E. Arzt, A. del Campo, *Adv. Mater.* **2010**, *22*, 2125.
[46] T. Xie, X. Xiao, *Chem. Mater.* **2008**, *20*, 2866.
[47] S. Reddy, E. Arzt, A. del Campo, *Adv. Mater.* **2007**, *19*, 3833.
[48] T. Meier, *Ph.D. Thesis*, Karlsruhe Institute of Technology **2014**.
[49] H. Hölscher, D. Ebeling, U. D. Schwarz, *Phys. Rev. Lett.* **2008**, *101*, 246105.
[50] H. A. Abdel-Aal, *J. Mech. Behav. Biomed. Mater.* **2018**, *79*, 354.
[51] D. L. Hu, J. Nirody, T. Scott, M. J. Shelley, *Proc. Natl. Acad. Sci. U. S. A.* **2009**, *106*, 10081.
[52] S. S. Sharpe, S. A. Koehler, R. M. Kuckuk, M. Serrano, P. A. Vela, J. Mendelson, III, D. I. Goldman, *J. Exp. Biol.* **2015**, *218*, 440.
[53] L. Mahadevan, S. Daniel, M. K. Chaudhury, *Proc. Natl. Acad. Sci. U. S. A.* **2004**, *101*, 23.
[54] W. Wu, L. Cheng, S. Bai, Z. L. Wang, Y. Qin, *Adv. Mater.* **2012**, *24*, 817.
[55] S. Ben, J. Tai, H. Ma, Y. Peng, Y. Zhang, D. Tian, K. Liu, L. Jiang, *Adv. Funct. Mater.* **2018**, *28*, 1706666.
[56] Z. Yang, J. K. Park, S. Kim, *Small* **2018**, *14*, 1702839.
[57] R. Nishimura, A. Fujimoto, N. Yasuda, M. Morimoto, T. Nagasaka, H. Sotome, S. Ito, H. Miyasaka, S. Yokojima, S. Nakamura, B. L. Feringa, K. Uchid, *Angew. Chem. Int. Ed.* **2019**, *58*, 13308.
[58] P. Fairley, *IEEE Spectrum* **2020**, *57*, 8.
[59] R. Leach, C. Giusca, M. Guttmann, P.-J. Jakobs, P. Rubert, C. Ann, *CIRP Ann.* **2015**, *64*, 545.
[60] S. Schauer, M. Worgull, H. Holscher, *Soft Matter* **2017**, *13*, 4328.
[61] S. Schauer, J. J. Baumberg, H. Holscher, S. K. Smoukov, *Macromol. Rapid Commun.* **2018**, *39*, 1800518.
[62] T. Meier, J. Bur, M. Reinhard, M. Schneider, A. Kolew, M. Worgull, H. Hölscher, *J. Micromech. Microeng.* **2015**, *25*, 065017.
[63] S. Schauer, X. Liu, M. Worgull, U. Lemmer, H. Hölscher, *Opt. Mater. Express* **2015**, *5*, 576.
[64] M. Worgull, *Hot Embossing: Theory and Technology of Microreplication (Micro and Nano Technologies)*, Elsevier Science, Norwich **2009**.
[65] A. Kolew, D. Münch, K. Sikora, M. Worgull, *Microsyst. Technol.* **2010**, *17*, 609.
[66] U. D. Schwarz, P. Köster, R. Wisesendanger, *Rev. Sci. Instrum.* **1996**, *67*, 2560.